JOURNAL OF GEOPHYSICAL RESEARCH, VOL. 112, C02011, doi:10.1029/2006JC003701, 2007

Shoaling and shoreline dissipation of low-frequency waves

A. van Dongeren,[1] J. Battjes,[2] T. Janssen,[2,3] J. van Noorloos,[2,4] K. Steenhauer,[2,5] G. Steenbergen,[2] and A. Reniers[2]

Received 12 May 2006; revised 25 August 2006; accepted 3 October 2006; published 13 February 2007.

[1] The growth rate, shoreline reflection, and dissipation of low-frequency waves are investigated using data obtained from physical experiments in the Delft University of Technology research flume and by parameter variation using the numerical model Delft3D-SurfBeat. The growth rate of the shoaling incoming long wave varies with depth with an exponent between 0.25 and 2.5. The exponent depends on a dimensionless normalized bed slope parameter β, which distinguishes between a mild-slope regime and a steep-slope regime. This dependency on β alone is valid if the forcing short waves are not in shallow water; that is, the forcing is off-resonant. The β parameter also controls the reflection coefficient at the shoreline because for small values of β, long waves are shown to break. In this mild-slope regime the dissipation due to breaking of the long waves in the vicinity of the shoreline is much higher than the dissipation due to bottom friction, confirming the findings of Thomson et al. (2006) and Henderson et al. (2006). The energy transfer from low frequencies to higher frequencies is partly due to triad interactions between low- and high-frequency waves but with decreasing depth is increasingly dominated by long-wave self-self interactions, which cause the long-wave front to steepen up and eventually break. The role of the breaking process in the near-shore evolution of the long waves is experimentally confirmed by observations of monochromatic free long waves propagating on a plane sloping beach, which shows strikingly similar characteristics, including the steepening and breaking.

Citation: van Dongeren, A., J. Battjes, T. Janssen, J. van Noorloos, K. Steenhauer, G. Steenbergen, and A. Reniers (2007), Shoaling and shoreline dissipation of low-frequency waves, *J. Geophys. Res.*, *112*, C02011, doi:10.1029/2006JC003701.

1. Introduction

[2] Short waves, with periods of O(10 s), incident on a beach force longer-period waves (O(100 s)), which are released from the short-wave groups in the shoaling and breaking process. These low-frequency (hereinafter LF) waves, also known as subharmonic gravity waves or infragravity waves, (partially) reflect off the beach, propagate seaward, and may become trapped at the coastline as edge waves or propagate out to deeper water as leaky waves. These waves can contain a significant portion of the total energy in the nearshore zone (e.g., *Wright et al.* [1979] and many studies thereafter) and are an important factor in the design of coastal structures in nearshore morphology and can induce low-frequency resonance in harbors [e.g., *Bowers*, 1977].

[3] The mechanism of the generation of infragravity waves has been studied for the last fifty years. *Biésel* [1952] and (independently) *Longuet-Higgins and Stewart* [1962, 1964] found that wave groups propagating over a horizontal bed force a second-order bound wave which is phase-locked and in antiphase with the short-wave envelope. Propagating over a sloping bed, the phase difference between the wave groups and the bound wave shifts away from 180 degrees, such that the long waves lag behind the wave groups This was shown from field data by *Masselink* [1985], numerically by *List* [1992] and theoretically by *Janssen et al.* [2003], who showed that for shoaling waves the bound wave travels slightly slower than the wave groups, which causes an increasing phase lag as the depth diminishes. This phase shift is crucial since it allows energy transfer from short waves to the bound long wave [*van Dongeren*, 1997] resulting in an amplitude growth stronger than conservative shoaling (Green's Law). Laboratory experiments [e.g., *Baldock et al.*, 2000], field data [e.g., *Elgar et al.*, 1992] and numerical studies [e.g., *Madsen et al.*, 1997; *van Dongeren*, 1997] showed that the shoaling rate of the incoming long-wave amplitude lies between Green's Law (amplitude increase proportional to $h^{-1/4}$) and the shallow-water equilibrium solution (amplitude increase proportional to $h^{-5/2}$) as a function of the ratio of the bed slope and the infragravity wave frequency.

[1] WL|Delft Hydraulics, Delft, Netherlands.
[2] Department of Civil Engineering, Delft University of Technology, Delft, Netherlands.
[3] Now at Department of Oceanography, Naval Postgraduate School, Monterey, California, USA.
[4] Now at Vopak, Vlaardingen, Netherlands.
[5] Now at Department of Engineering, King's College, University of Aberdeen, Aberdeen, UK.

0148-0227/07/2006JC003701$09.00

Table 1. Nondimensional β_b Parameter for Various Locations

Location	β_b
Monterey, California (USA)	0.25
Duck, North Carolina (USA)	0.2
Petten, Netherlands	0.08
Terschelling, Netherlands	0.1

[4] From an analysis of *Boers* [1996] laboratory data of irregular waves, *Battjes et al.* [2004] found that the shoaling of the incoming low-frequency wave is a function of the normalized bed slope parameter

$$\beta = \frac{h_x}{\omega}\sqrt{\frac{g}{h}}, \tag{1}$$

where h_x is the bed slope, ω is the radial frequency of the LF waves, g is the gravitational acceleration and h is a representative depth. *Battjes et al.* [2004] use a characteristic shelf depth h_s to calculate the normalized bed slope parameter (denoted by β_s). In the present paper we will use a characteristic breaking depth h_b instead (denoted by β_b). The β parameter is analogous to the surf similarity parameter or Iribarren parameter [*Battjes*, 1974] and the Symonds parameter [*Symonds et al.*, 1982]. *Battjes et al.* [2004] found from the data that for values of $\beta_s < 0.06$ (corresponding to $\beta_b < 0.1$), a "mild-slope regime" exists in which the amplitude growth in the shoaling zone is large. For values $\beta_s > 0.3$ or $\beta_b > 0.45$ (the "steep-slope regime"), the amplitude growth is weak.

[5] In the breaking region, the individual short waves start to dissipate owing to breaking. In this region and in the inner surf zone, infragravity wave generation can take place owing to the moving breakpoint [*Symonds et al.*, 1982] or owing to groupiness in the surf zone itself [*Foda and Mei*, 1981; *Schäffer and Svendsen*, 1988]. *Van Dongeren et al.* [2002] showed that the ratio of shoaling zone forcing to surf zone forcing (the sum of generation by moving breakpoint and inner surf zone forcing) is inversely proportional to β_b. For values of β_b found for typical beaches in the U.S. (Duck, NC and Monterey, CA) and the Netherlands (Petten and Terschelling) shoaling-zone forcing dominates surf zone forcing (Table 1).

[6] *Battjes et al.* [2004] found that β also governs dissipation at the shoreline. While for large values of β long waves are nearly fully reflected from the shoreline, for small values of β ($\beta_s < 0.06$, mild-slope regime) reflections at the shoreline are small. They showed that the conventional criterion used to distinguish breaking and nonbreaking short waves on a slope also applies to low-frequency waves near the shoreline, on the basis of which they postulated that the observed energy losses are due to the breaking of the long waves. This hypothesis was further substantiated by *van Dongeren et al.* [2004] in a preliminary analysis of the experimental data also used in the present paper. Alternative dissipation mechanisms were presented by *Henderson and Bowen* [2002], who had attributed (with some reservations) the observed shoreline dissipation of long-wave energy to bottom friction. However, *Henderson et al.* [2006] showed that this was not the cause and proposed a nonlinear transfer mechanism through triad interactions from LF energy to high-frequency energy instead.

[7] Few laboratory or numerical experiments have been performed to study the infragravity wave generation (in the shoaling zone) and dissipation mechanisms (at the shoreline) in detail. *Kostense* [1984] only measured the amplitudes of the incoming and outgoing long waves on the horizontal part in front of a sloping beach. *Baldock et al.* [2000] studied breakpoint forced waves on a very steep beach (1:10) for large β values. *Janssen et al.* [2000] performed measurements with high spatial resolution in the surf zone but limited to short durations and without second-order wave generation or active reflection compensation. *Boers* [1996] did use higher-order wave control but studied only irregular waves on a barred beach. *Baldock and O'Hare* [2004] found a transfer of energy from the primary wave components to subharmonics and superharmonics in the surf zone, and an amplitude reduction of the long-wave motion, which commenced at the breakpoint.

2. Objectives and Outline of the Paper

[8] The objectives of this paper are to verify and extend the findings from *Battjes et al.* [2004] by analyzing the growth rate of the incoming long waves, their shoreline reflection properties and shoreline dissipation mechanism.

[9] In section 3 we describe a new data set with a very high spatial resolution from laboratory experiments with bichromatic waves conducted on a plane sloping beach. In addition to the laboratory experiments, the influence of variations in parameters of bed slope, difference frequency, short-wave amplitude and steepness, and offshore depth has been investigated using the one-dimensional mode of the Delft3D-SurfBeat model [*Roelvink*, 1993]; see section 4.

[10] After decomposition of the total LF signal into incoming and reflected long-wave components (Appendix A), the shoaling rate as a function of the normalized bed slope parameter is analyzed in section 5, while the shoreline reflection and dissipation are investigated in sections 6 and 7. A preliminary analysis of this data was presented by *van Dongeren et al.* [2004].

3. Laboratory Experiments

[11] The laboratory experiments have been performed in the Long Research Flume in the Fluid Mechanics Laboratory of the Department of Civil Engineering at the Delft University of Technology (TU Delft). The flume is 40 meters long and is equipped with a high-accuracy Rexroth/Hydraudyne wave maker with WL|Delft Hydraulics second-order wave generation and Active Reflection Compensation (ARC), which minimizes reflections from the wave maker. We refer to the work of *van Noorloos* [2003] for details.

[12] An impermeable smooth concrete beach with a 1:35 slope was constructed. The toe of the beach was located at 8.5 meters from the wave maker. Wave experiments were run with a still water depth of 0.70 m over the horizontal approach (Figure 1).

[13] The experimental program of the bichromatic wave conditions is given in Table 2. The bichromatic experiments

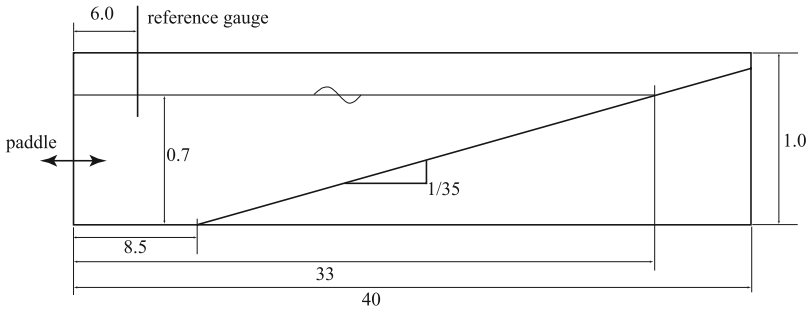

Figure 1. Side view of the experimental setup. Distances are in meters. From *van Noorloos* [2003].

were run for 10 minutes including ramp-up time, which yields an effective record length of about 5 minutes.

[14] Waves were measured using 11 wave gauges at a sample rate of 25 Hz. Each experiment was run eight times for different wave gauge locations. The eight sessions were combined and synchronized into one data set with records from 80 wave gauge locations for each experiment with a resulting resolution of 0.5 m in the shoaling zone and 0.3 m in the surf zone (bottom panel of Figure A1).

[15] In the experiments labeled "A" the frequencies of the primary components f_1 and f_2 were varied, such that the difference between the two (the difference frequency) as well as the β parameter was varied but the mean frequency was kept constant. In series B the amplitude of the f_2 component and consequently the modulation and the amplitude of the generated incoming bound long wave was varied. The departure from resonance for the LF forcing, measured by

$$\mu_s = 1 - \frac{C_{g,s}^2}{gh_s}, \tag{2}$$

is roughly *O(1)* in the shoaling region for all laboratory cases. Here $C_{g,s}$ is the group speed of the mean primary wave frequency at a representative depth h_s in the shoaling region. Therefore we consider the forcing to be off-resonant in the shoaling regime and assume the long-wave evolution in that region to be governed by the relative bottom slope β alone [*Battjes et al.*, 2004].

4. Variation of Parameters With Delft3D-SurfBeat

[16] The experimental results from the laboratory were extended with results from the numerical model Delft3D-SurfBeat [*Roelvink*, 1993], which solves the one-dimensional short-wave averaged mass and momentum equations with radiation stress forcing. The forcing is calculated from the group-resolving energy equation of the short waves which is integrated concurrently. The energy equation accounts for bottom friction dissipation [*Putnam and Johnson*, 1949] with an estimate of the friction factor by *Swart* [1974]. Dissipation due to depth-induced wave breaking is modeled on the basis of a modification of the *Battjes and Janssen* [1978] model. We refer to the work of *Steenhauer* [2003] for details on the numerical experiments.

[17] The following parameters were varied in the numerical experiments: beach slope, difference frequency, offshore (shelf) depth, short-wave modulation and primary wave amplitude, see Tables 3–8 for details. As for the physical experiments, for the numerical experiments the LF forcing is off-resonant in the shoaling regime ($\mu \sim$ O(1)), with the notable exception of case D-1 where the forcing is near-resonant [*Janssen et al.*, 2003], which will be shown to be a special case in the next section.

[18] The numerical experiments were run on a model grid with the same layout (horizontal shelf and plane slope) as the physical model with a grid resolution of 0.33 m. The time step is 0.1 s, so that the maximum Courant number is

$$C_r = \sqrt{gh}\frac{\Delta t}{\Delta x} = 0.8. \tag{3}$$

[19] At the wave-maker boundary, the time variation of the energy on the wave group scale is specified and is computed as follows. Utilizing the frequency and amplitude from Tables 3–8, a realization of the short-wave surface elevation η at the wave maker is constructed. The squared surface elevation averaged over the short-wave period is proportional to the group-varying energy as

$$E = \rho g\overline{\eta^2} = \frac{1}{2}\rho g A^2, \tag{4}$$

in which A is the time-varying amplitude of the surface elevation (the short-wave envelope). Also specified at the location of the wave maker is the time-varying set-down. The wave-maker boundary is a weakly reflecting boundary that allows waves propagating from the shore to the boundary to leave the domain with a minimum of reflection [*Roelvink*, 1993]. The shoreline boundary allows for time-varying run-up [*Roelvink*, 1993] and the lateral boundaries

Table 2. Bichromatic Wave Conditions in Physical Experiment[a]

ID	f_1, Hz	f_2, Hz	Δf, Hz	a_1, m	a_2, m	β_b	δ	Symbol
A-1	0.6714	0.4761	0.1953	0.06	0.012	0.16	0.2	plus
A-2	0.6470	0.5005	0.1465	0.06	0.012	0.22	0.2	plus
A-3	0.6348	0.5127	0.1221	0.06	0.012	0.25	0.2	plus
A-4	0.6226	0.5249	0.0977	0.06	0.012	0.32	0.2	plus
B-1	0.6470	0.5005	0.1465	0.06	0.018	0.21	0.3	square
B-2	0.6470	0.5005	0.1465	0.06	0.024	0.21	0.4	square
B-3	0.6470	0.5005	0.1465	0.06	0.03	0.21	0.5	square
B-4	0.6470	0.5005	0.1465	0.06	0.036	0.20	0.6	square

[a]The modulation factor δ is the ratio a_1 over a_2.

Table 3. Bichromatic Wave Conditions in Numerical Simulations in Addition to the Conditions in Table 2[a]

ID	f_1, Hz	f_2, Hz	Δf, Hz	a_1, m	a_2, m	β_b	δ
A-5	0.5945	0.5529	0.042	0.06	0.012	0.76	0.2
A-6	0.5859	0.5615	0.024	0.06	0.012	1.28	0.2

[a]The symbol used in the figures is a plus.

Table 4. Bichromatic Wave Conditions in Numerical Simulations in Addition to the Conditions in Table 2 With a Varying Bed Slope[a]

ID	h_x	β_b
C-1	1/10	0.89
C-2	1/20	0.44
C-3	1/30	0.30
C-4	1/40	0.22
C-5	1/50	0.18
C-6	1/60	0.15
C-7	1/70	0.13

[a]Other conditions are as those in experiment A-3. The symbol used in the figures is a cross.

Table 5. Bichromatic Wave Conditions in Numerical Simulations in Addition to the Conditions in Table 2 With a Varying Bed Slope[a]

ID	h_x	β_b
C-8	1/10	4.43
C-9	1/15	2.96
C-10	1/20	2.23
C-11	1/30	1.48
C-12	1/40	1.11

[a]Other conditions are as those in experiment A-6. The symbol used in the figures is a cross.

Table 6. Bichromatic Wave Conditions in Numerical Simulations in Addition to the Conditions in Table 2 With a Varying Bed Slope and Very Small β_b Values[a]

ID	h_x	f_2, Hz	Δf, Hz	β_b
C-13	1/50	0.3906	0.1953	0.082
C-14	1/60	0.3906	0.1953	0.072
C-15	1/70	0.3906	0.1953	0.086

[a]Other conditions are as those in experiment A-6. The symbol used in the figures is a cross.

Table 7. Bichromatic Wave Conditions in Numerical Simulations in Addition to the Conditions in Table 2 With a Varying Offshore Depth h_0 With Other Conditions as in Experiment A-2[a]

ID	h_0, m
D-1	0.4
D-2	1.0
D-3	1.5
D-4	2.0
D-5	2.5

[a]The symbol used in the figures is a circle.

Table 8. Bichromatic Wave Conditions in Numerical Simulations in Addition to the Conditions in Table 2 With Varying Short-Wave Amplitude With Other Conditions as in Experiment A-2[a]

ID	$a_1 = a_2$, m
E-1	0.036
E-2	0.039
E-3	0.042
E-4	0.045
E-5	0.048

[a]The symbol used in the figures is a diamond.

are straight, impermeable walls, which mimics the glass walls in the flume. The initial condition is still water.

5. Growth Rate of Shoaling Incoming Long Waves

[20] The measured signals are first decomposed into incoming and reflected waves using subarrays of adjacent wave gauges (Appendix A). After this decomposition the growth rate of the amplitude of the incoming long waves can be evaluated by fitting a function of local depth with an unknown power α to the observed amplitude variation as

$$\hat{\varsigma} \sim h^{-\alpha} \tag{5}$$

in the shoaling region between $x = 8$ m and $x = 25$ m. This is done for all numerical and physical experiments. The results (Figure 2) show that the exponent decays sharply with increasing β_b from the value of around 1.8 at $\beta_b \approx 0.08$ to a value of 0.25 (Green's Law, conservative shoaling) for the case of relatively steep normalized slopes. The experiments were conducted for cases with μ values in a range such that the short waves propagate in intermediate depth. This means that, as β_b approaches zero, the exponent α will have a value less than 2.5 (the shallow water limit [*Longuet-Higgins and Stewart*, 1962, 1964]).

[21] The numerical results for the same parameter settings (cases A and B) give a 25% higher shoaling rate than the physical experiment results. While the short-wave height variation is predicted well by the numerical model (not shown), the energy transfer from short waves to long waves is not. The reason for this mismatch is not clear. Nevertheless, the trend is predicted well by the numerical model, and we will use these results in the remainder.

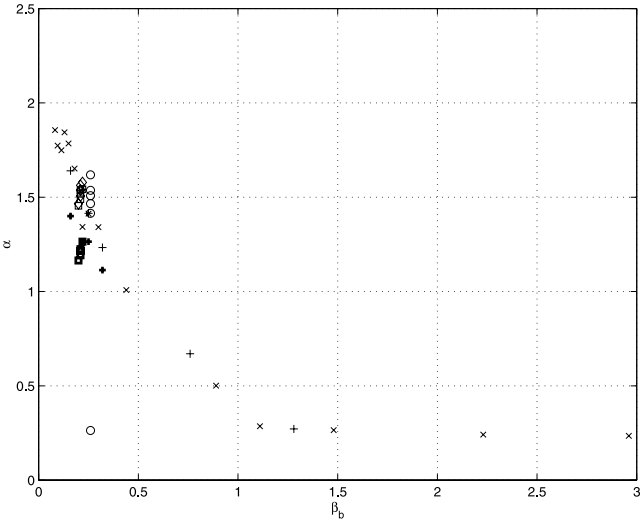

Figure 2. Growth rate α as a function of β_b analyzed from the physical (bold symbols) and numerical experiments (thin symbols) with the following parameter variations: circles indicate variation of offshore depth; pluses indicate variation of difference frequency; crosses indicate variation of bed slope; squares indicate variation of short-wave modulation; and diamonds indicate variation of short-wave amplitude.

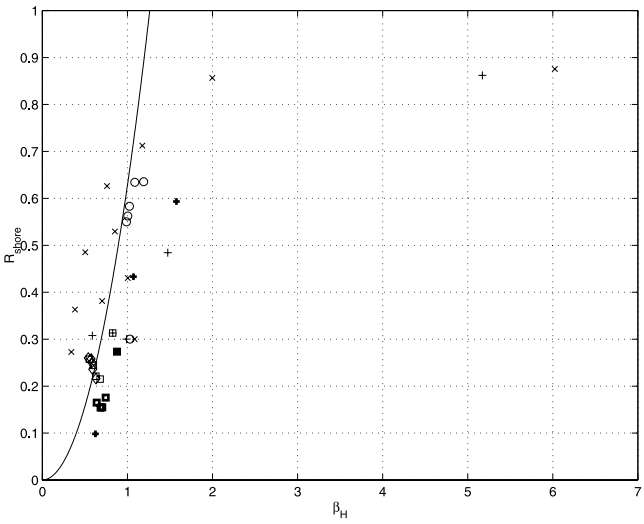

Figure 3. Shoreline reflection coefficient R as a function of β_H. Equation (8) is plotted as the solid line. The other symbols are the same as those in Figure 2.

[22] Relative to this trend, there is some variation with the other parameters. The variation due to the short-wave modulation (series B) and the short-wave amplitude (series E) is rather small. A doubling of the modulation results in only a ten percent increase in shoaling rate in both cases. The offshore depth can have a large effect on the resulting growth rate (series D). If the depth is large enough such that the primary waves propagate in intermediate to deep water, the variation of the shoaling rate is small relative to the variation of the offshore depth. However, when the offshore depth is small, μ (equation (2)) is not small and the short waves themselves propagate in shallow water already (the near-resonant case of *Janssen et al.* [2003]). If the wave field is then initiated with second-order uniform-depth theory the forcing is only very slowly pushed away from quadrature such that, over typical propagation lengths in the laboratory, energy transfers will be minimal and the long waves shoal almost according to Green's Law, see the circle at (β_b,α = 0.25, 0.25).

[23] Despite the slight dependence on other parameters, and for a sufficient offshore depth such that the interaction is indeed off-resonant in the shoaling region, these results confirm the findings by *Battjes et al.* [2004] that the β parameter is the major controlling parameter for the shoaling behavior. The present results further illustrate that while the variation is gradual, it is possible to define a mild-slope and a steep-slope regime, albeit that these results would suggest the mild-slope regime in the range $\beta_b < 0.3$ and the steep-slope regime in the range of β_b exceeding a value of about 1, where there is a transition to conservative shoaling (α = 0.25).

6. Shoreline Reflection

[24] Besides governing the shoaling of the incoming long wave, the β parameter also seems to control shoreline dissipation. This hypothesis can be substantiated from the present data sets by plotting the reflection coefficient as a function of the local β parameter.

[25] We define the shoreline reflection coefficient as the ratio of the amplitude of the reflected wave to that of the incoming wave at the shorewardmost subarray (see Appendix A). This is in only a few centimeters of still-water depth. The area beyond this point includes therefore practically only the swash zone.

[26] The reflection coefficient is plotted in Figure 3 against β_H, which is defined as

$$\beta_H = \frac{h_x}{\omega}\sqrt{\frac{g}{H}}\,, \tag{6}$$

in which H is the wave height of the incoming long wave near the shoreline (in the center of the shorewardmost array). The graph shows a clear dependency of the reflection on β_H. This parameter is directly related to the surf similarity parameter ξ as

$$\xi = \sqrt{2\pi}\beta_H. \tag{7}$$

[27] For short waves, *Battjes* [1974] found a relation between the reflection coefficient at the shoreline R and the surf similarity parameter, which can be rewritten using equation (7) as

$$R = 0.1\xi^2 = 0.2\pi\beta_H^2\,. \tag{8}$$

[28] This relationship (solid line in Figure 3) appears to also apply to low-frequency waves, albeit that there is considerable scatter. Again, there is a transition, now at $\beta_H \approx 1.25$, similar to the value found previously for the onset of breaking of short waves [*Battjes*, 1974].

[29] Analysis of field data (see, e.g., the work of *Sheremet et al.* [2002], *Elgar et al.* [1994], and older references therein) has not shown a reflection coefficient at the shoreline of the LF waves of much less than unity. In the case of *Elgar et al.* [1994] this is owing to the fact that instruments were not located close to the shoreline but outside the surf zone. While propagating from the sensors to the shoreline and back, the infragravity waves can still be gaining energy in the surf zone. *Sheremet et al.* [2002] did have sensors close to the shoreline and still measured reflection coefficients at the shoreline of about unity. In his case the local beach slope at the shoreline was very steep (1/20). For the high-frequency end of the low-frequency range they considered (0.05 Hz) and the low-frequency wave height of 0.22 m (calculated from his Figure 3c), we find β_H = 1.1, which corresponds to a reflection coefficient of 0.76. For a frequency in the middle of the regime (f = 0.03 Hz) we obtain β_H = 1.8 and the reflection coefficient is unity. The bulk reflection coefficient over the entire range will then also be close to unity.

[30] *Okihiro and Guza* [1995] did find a dependency of the reflection coefficient on the tidal level. While in this case the sensors were also well outside the surf zone, they ascribed this effect in part to the more complete reflection on the high-tide (steeper) beach face. However, in a follow-up study, *Thomson et al.* [2006] found from field data that variation of the ratio of reflected and incoming LF energy was not due to incomplete reflection but rather to nonlinear

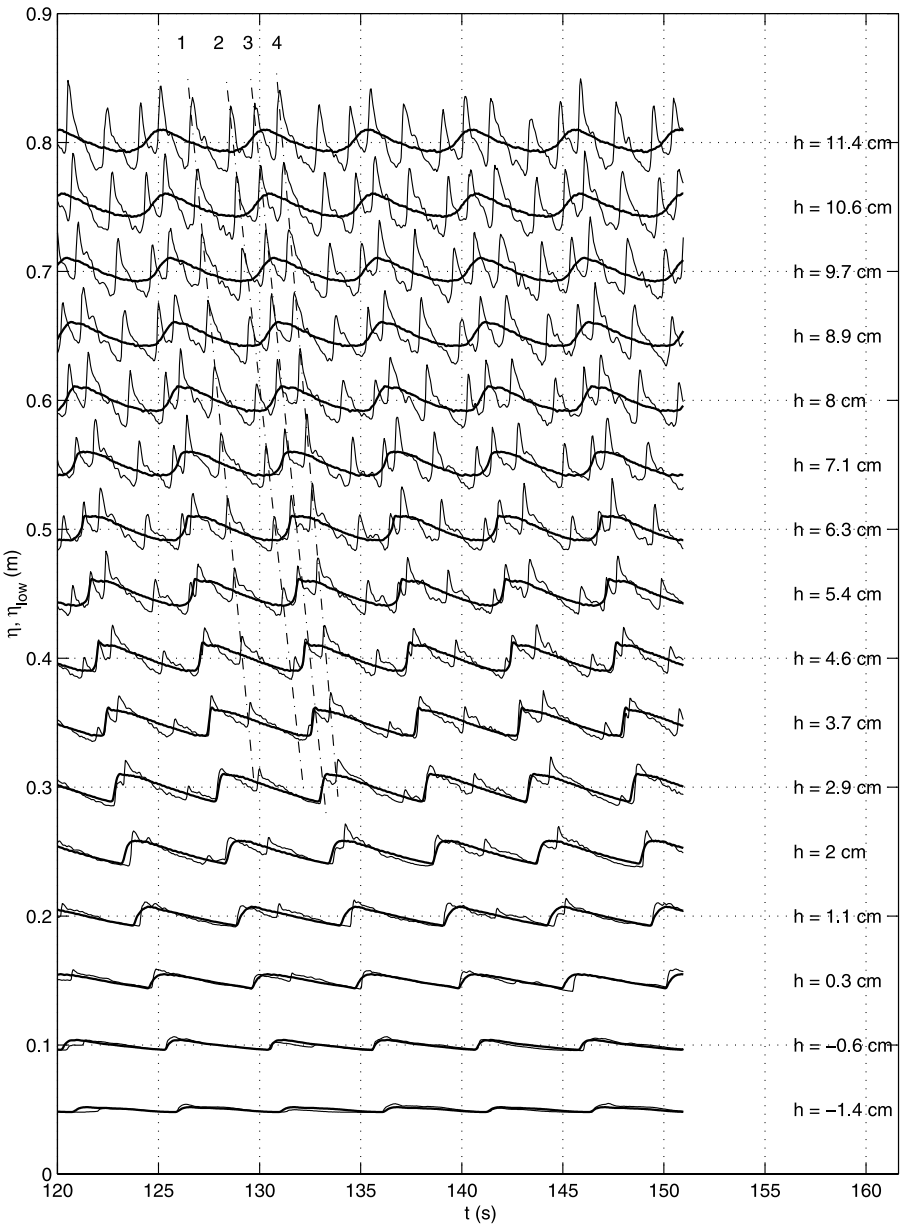

Figure 4. Time series of the filtered (low-frequency component and its higher harmonics) long wave (thick solid line), and total measured time series (thin solid line) for consecutive gauge positions around the still water line for case A-1. Tracks of converging wave crests are shown as dash-dotted lines.

energy transfer to higher frequencies in the inner surf zone very near to the shoreline. We will discuss this mechanism in the next section. Their finding of full reflection from the shoreline seems inconsistent with the present findings. However, we define our reflection coefficient in about 3 centimeters of water depth, which would represent about 30 centimeters of depth or 15 meters from the shoreline, scaled to the field site that *Thomson et al.* [2006] investigated. The squared reflection coefficient they find at that location is about 0.2, judging from their Figure 2a or $R = 0.44$, which is close to $R = 0.32$, which we calculate from equation (8) using $f = 0.03$ Hz, $h_x = 0.02$, $H_{m0,low} = 0.22$ m (calculated from their Figure 2a). It must be noted that the reflection coefficients found in these field experiments may be difficult to interpret because of the sparseness of the measurement array. The above shows that while reflection coefficients less than unity have not in fact been measured, they may occur in the field.

7. Shoreline Dissipation Mechanism

[31] Figure 3 shows that the reflection coefficient at the shoreline is much less than unity for small values of the normalized bed slope parameter, which suggests that there is some kind of dissipation which may also be a function of this parameter. In this section, we will show that this dissipation is due to long-wave breaking for small values of β.

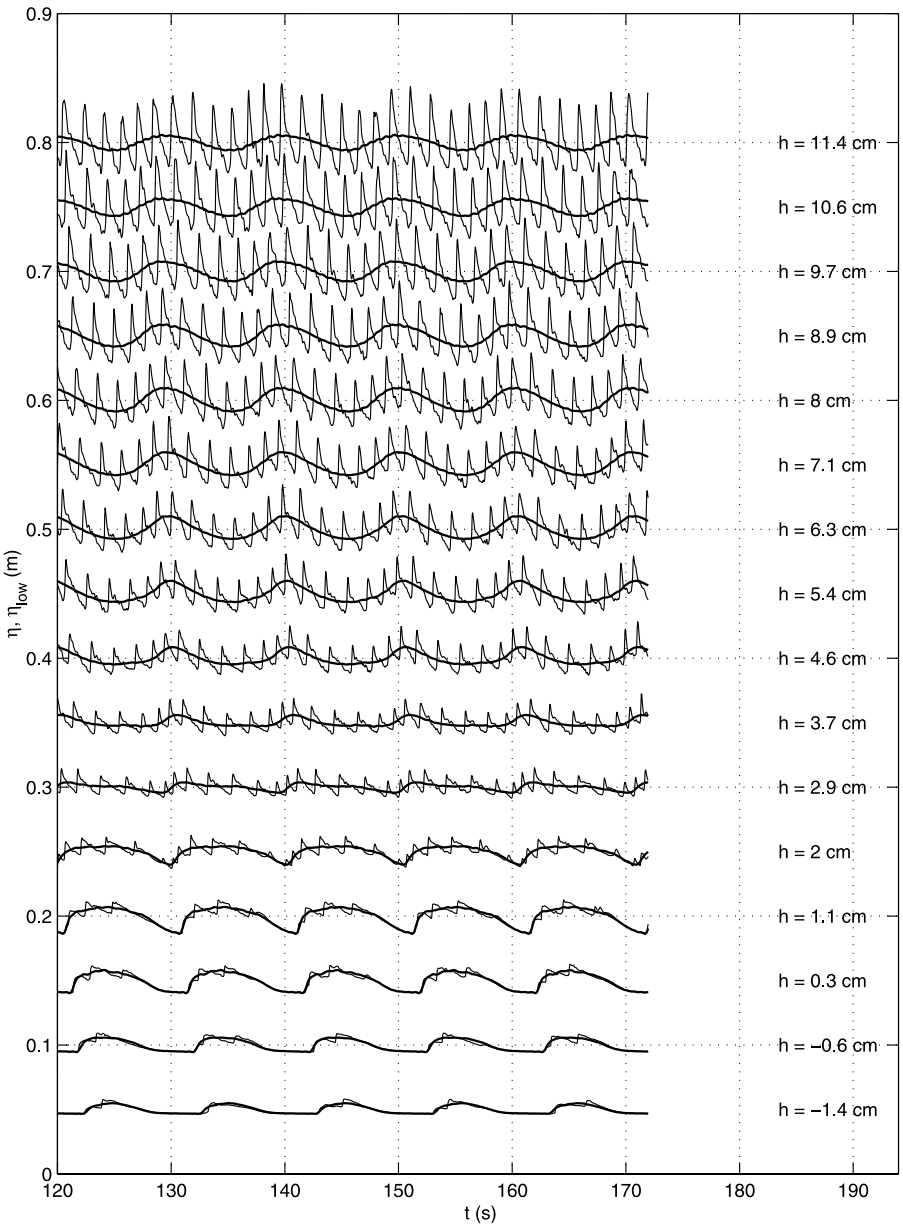

Figure 5. Same as Figure 4 but for case A-4.

[32] Surface elevation records obtained in the laboratory for one bichromatic case (case A-1 with $\beta_b = 0.16$) have been filtered in the Fourier domain such that only the difference frequency ($\Delta f \equiv f_1 - f_2$) between the primary wave components and integer multiples of this difference frequency ($m\Delta f$, where the integer $m = 2..f_{nyq}/\Delta f$) remain. (As will be shown below, the variance at $m\Delta f$ frequencies is mostly due to self-self interactions of the difference frequency and not due to interactions of higher-frequency components.) The primary wave components themselves, their superharmonics, and components due to triad interactions between the primary components and the difference frequency are filtered out. This filtering has been performed on the measured wave data (not decomposed into incoming and reflected components) from the gauges closest to the shoreline.

[33] Figure 4 shows the filtered time traces (thick solid lines) for various cross-shore locations (including some shoreward of the still-water line) as well as the total (unfiltered) time traces (thin solid lines). The filtered time series show that the long wave steepens-up to a bore-like front (in depths $h > 3$ cm) and then decays (in depths $h < 3$ cm), resembling short-wave breaking. The dash-dotted line marked with the "1" indicates a short-wave crest in the total time series which rides on the lee side of the long wave and which is seen to propagate by itself. In contrast, the other dash-dotted lines (marked "2," "3," and "4") indicate a triplet of wave crests on either side of the long-wave front, which are seen to converge on the long-wave bore front. This is because a short wave just behind the bore propagates in deeper water and experiences a following "current" induced by the long wave and will therefore slowly catch up with the bore. A wave just in front of the

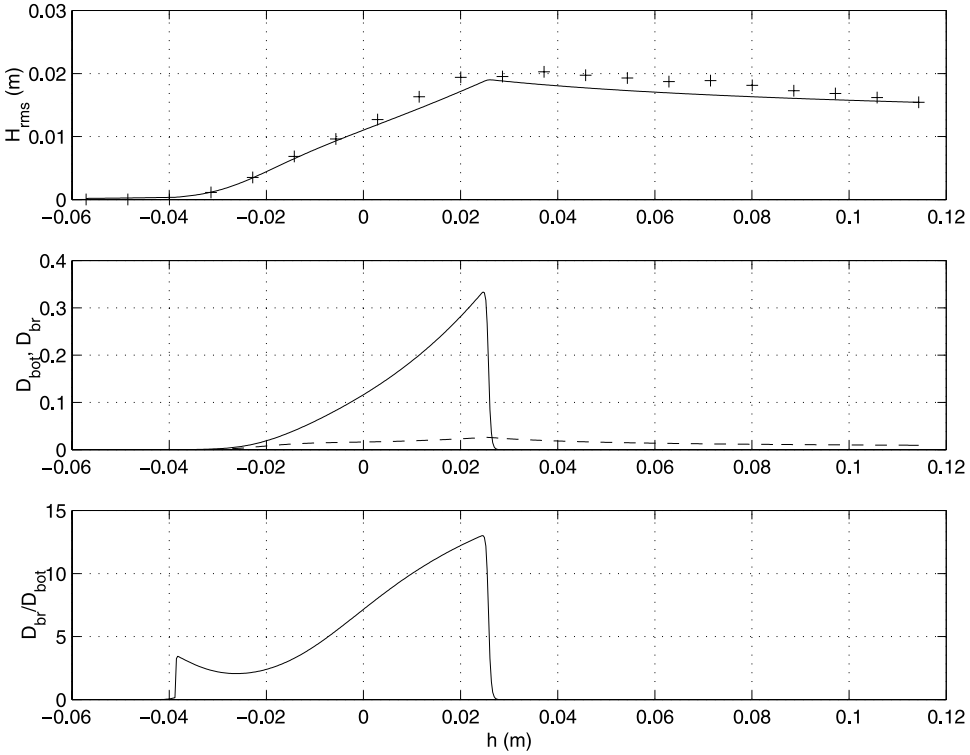

Figure 6. (top) Low-frequency wave heights as a function of still water depth (solid line shows the energy model; pluses are measurements). The dry beach is to the left. (middle) Dissipation due to breaking (solid line) and due to bottom friction (dashed line). (bottom) Local ratio of the two local dissipation rates.

bore will propagate in shallower water and experience an opposing "current" and be caught. This pattern of "single" wave decay, and "twin" or "triple" wave convergence can be seen in the entire time series and reduces the number of short waves as the depth decreases. This pattern of bore-bore capture of short waves has been previously reported by, for example, *Sénéchal et al.* [2001].

[34] For small water depths $h \leq 4.6$ cm the fronts of the breaking long waves coincide with (i.e., are part of) fronts of the breaking short waves owing to the convergence described above. It can also be seen that the highest short waves "ride" on top of the long-wave crests, which illustrates the positive correlation between the short-wave envelope and the long waves near the shoreline as found by, for example, *Janssen et al.* [2003]. Another way to view this is that the highest short waves can only exist when the local water depth is temporarily increased under a long-wave crest. This filtering effect of the long wave on the short-wave heights may have an important effect on the wave attack of structures and dunes [e.g., *Kamphuis*, 1996].

[35] The results for cases A-2 and B-1 through B-4 show similar patterns of long-wave steepening and dissipation as depicted in Figure 4 and are not shown. In the case of A-3 and A-4 the shoreline reflection is stronger and the filtered signal (thick solid line, Figure 5) exhibits no evidence of long-wave steepening and breaking with the short waves (thin solid line) propagating over the modulated mean water level.

[36] The suggestion from Figure 4 is that steepening of the wave fronts and then long-wave breaking (and not bottom friction) is the likely dissipation agent (for small values of the normalized bed slope parameter). This can be substantiated by considering the cross-shore energy equation for linear, shoreward-propagating long waves:

$$\frac{d}{dx}\left(\sqrt{gh}\frac{1}{8}\rho g H_{rms,lo}^2\right) = -D_{bot} - D_{br}, \tag{9}$$

where ρ is the density and D_{bot} and D_{br} are terms that account for dissipation of wave energy due to bottom friction and breaking, respectively. The dissipation rate due to breaking [*Battjes and Janssen*, 1978] is modeled as

$$D_{br} = \alpha_{br} f_{low} \rho \;\; g\frac{H_{rms,lo}^2}{4}, \tag{10}$$

where α_{br} is a tuning parameter. Here we have assumed that the presence of high-frequency waves does not influence the rate at which breaking dissipates long-wave energy. Following *Henderson and Bowen* [2002], the bottom friction dissipation rate is modeled as

$$D_{bot} = f_{cw}\rho\left(\frac{g}{h}\right)^{3/2}\frac{H_{rms}}{\sqrt{8}}\frac{H_{rms,lo}^2}{8}, \tag{11}$$

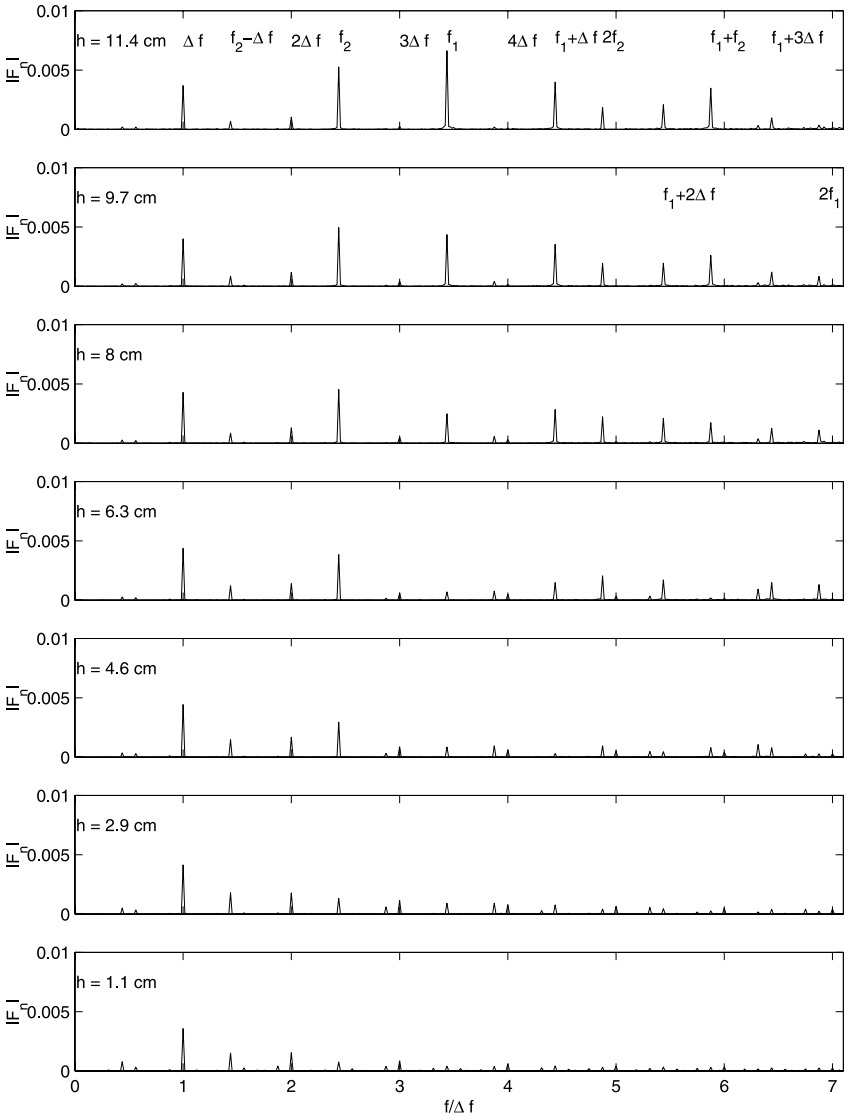

Figure 7. Frequency spectra of case A-1 at various depths. The most important frequency components are indicated in the first and second panels. The frequency axis is normalized by $\Delta f = 0.1953$ Hz.

where f_{cw} is the friction coefficient, and where we have relaxed the assumption of weak low-frequency motions by using H_{rms} instead of $H_{rms,hi}$. The ratio of the two mechanisms yields

$$\frac{D_{br}}{D_{bot}} = \frac{2\sqrt{8}\alpha_{br}}{f_{cw}\gamma_b} f_{low}\sqrt{\frac{h}{g}} \qquad h \le h_{b,low}, \tag{12}$$

where $\gamma_b = H_{rms}/h$ is the breaking index for the short waves. The equation shows that dissipation due to breaking becomes more important than bottom friction dissipation for large values of the frequency f_{low}. Using typical parameter values $\alpha_{br} = 1$, $f_{cw} = 0.015$ (using *Swart* [1974]), and

$$\gamma_b = 0.29 + 0.76kh \tag{13}$$

[*Ruessink et al.*, 2003], the result for case A-1 is shown in Figure 6. The modeled long-wave height transformation (solid line, top panel) resembles the energy decay calculated directly from the measurements (+), and shows the importance of a sudden enhancement of spatial decay due to breaking rather than a gradual decay due to bottom friction. The dissipation due to bottom friction occurs in the entire domain, but at a relatively low rate (middle panel, dashed line). The dissipation due to breaking is much larger (middle panel, solid line) in the region where the long waves break. The bottom panel shows the ratio of the two dissipation rates. Locally, dissipation due to breaking is almost 20 times larger than the dissipation due to friction. Integrated cross-shore, the ratio of breaker dissipation over bottom friction dissipation is about 4.7 for this case.

[37] This confirms the work of *Henderson et al.* [2006] and *Thomson et al.* [2006], who also concluded that bottom friction is not the agent for LF energy dissipation. Instead they attribute energy losses in the low-frequency spectral range to energy transfer to the swell spectral range through quadratic nonlinear coupling. In the present analysis (where

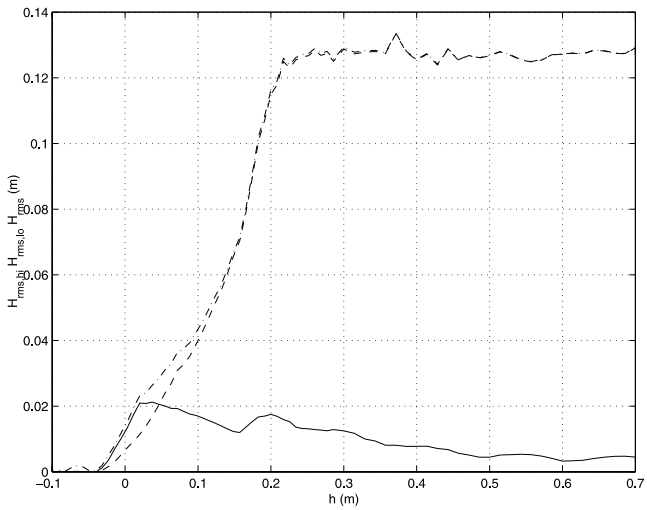

Figure 8. Measured H_{rms} wave heights (solid line shows low-frequency; dashed line shows high-frequency; and dash-dotted line shows total) as a function of still water depth.

the primary frequencies represent the "swell" frequencies) we also find that nonlinear effects are important for the long-wave evolution in the surf zone. However, instead of an interaction with the swell field directly as in the work of *Henderson et al.* [2006], we particularly consider the self-self interaction of the long waves (which were not considered by *Henderson et al.* [2006]). These interactions result in enhancement of the long-wave harmonics, associated with the steepening of the LF wave front (which starts at a depth of about 10 centimeters, Figure 4), and the eventual breaking of the long wave.

[38] To illustrate this further, we refer to frequency spectra of the measured data at various depths (Figure 7), which show that besides the primary components f_1 and f_2, with their higher harmonics, and the difference frequency Δf with its integer multiples, there are other components present which are, for example, due to triad interactions between f_1, f_2 and Δf, most notably $f_2 - \Delta f$ and $f_1 + \Delta f$. However, including, for example, the $f_2 - \Delta f$ harmonic in the filtered time series slightly changes the lee side of the LF waves but not the bore-like front (not shown).

[39] Since breaking dissipation is initially more effective in the more energetic higher frequency ranges, the primary components f_1, f_2 and their higher harmonics dissipate (Figure 7) and in very shallow water long-wave motion dominates the wave field (in case A-1 this happens around h = 5 cm; see also Figure 8). As a consequence, the nonlinear coupling to the swell waves in shallow water is relatively weak (Figure 7, bottom panels), while the components due to self-self interactions become dominant there. This indicates that the variance at integer multiples of the difference frequency is primarily due to self-self interactions of the LF-waves and not due to interactions between higher-frequency components (e.g., the energy at $2\Delta f$ is mostly the result of the self-self interaction $\Delta f + \Delta f$ and not by $2f_1 - 2f_2$ or other difference contributions from the high-frequency field). Through these self-self interactions the long-wave fronts steepen on the slope until the waves become unstable and break; this shoaling process is in many ways similar to the nonlinear near-shore evolution of swell or wind waves on a beach. The mechanisms of nonlinear energy transfers through triad interactions between lf waves and swell, and self-self interactions of the LF-waves appear thus to coexist with the latter dominating in very shallow water, and being the ultimate physical mechanism for shallow-water energy losses in the lf ranges.

[40] To verify our inferences with respect to the nonlinear transfer mechanisms and long-wave dissipation in shallow water, we generated periodic (free) long waves in the flume (Figure 1) with Δf = 0.195 Hz (same as case A-1, see Table 2) and wave height of 0.01 m, thus a (free) wave at the same frequency as the lf waves in experiment A-1 but without the primary waves. The time traces (Figure 9) show that on the slope, and in shallow water, the initially sinusoidal long waves produce higher harmonics, steepen up and transition into turbulent bores. Most of the incident wave energy is dissipated and reflection of wave energy from the shoreline appears weak.

[41] Frequency spectra at various depths (Figure 10) show that only Fourier components at the free long-wave frequency and its higher harmonics contain significant variance, and that the distribution over the frequencies and spatial evolution is similar to the bichromatic wave case of Figure 7. Although the details of the breaking process of the free long waves are slightly different, the results are strikingly similar to the filtered results of Figures 4 and 7. These findings thus corroborate our conclusions with respect to the dominant role of self-self interactions of the LF-waves and the dissipation of long waves in the near-shore.

[42] Field evidence of shoreline breaking of LF waves is scarce. *Munk and Wimbush* [1969] showed that a breaker criterion similar to the one we use here could be successfully applied to long waves such as tsunamis and tides. *Nazaka et al.* [1990] investigated long waves breaking over a coral reef. *Ruessink et al.* [1998] showed that, for highly dissipative conditions at a beach in the Netherlands, the higher-frequency end of the infragravity wave spectra is saturated, which implies (long) wave breaking and a reflection coefficient of less than unity. Likewise, for a highly dissipative Oregon beach, *Ruggiero et al.* [2004] showed that the higher-frequency region of the run-up spectra (which variance was almost completely in the infragravity band) was saturated and that these spectra were dependent on beach slope, which indicates a dependence on β. As mentioned above, *Sénéchal et al.* [2001] presented evidence of the formation of wave fronts at the timescale of the low-frequency waves.

8. Conclusions

[43] In this paper a high-resolution data set is presented of bichromatic waves over an impermeable plane sloping beach. The LF waves are separated into incoming and reflected components using a multistep method, which allows for a correction of the a priori assumed phase velocity and accounts for shoaling (Appendix A).

[44] We find that the shoaling of the incoming long wave and dissipation at the shoreline have a mild-slope regime $\beta_b < 0.3$ and a steep-slope regime for $\beta_b > 1$. The growth rate of incoming waves is strongly dependent

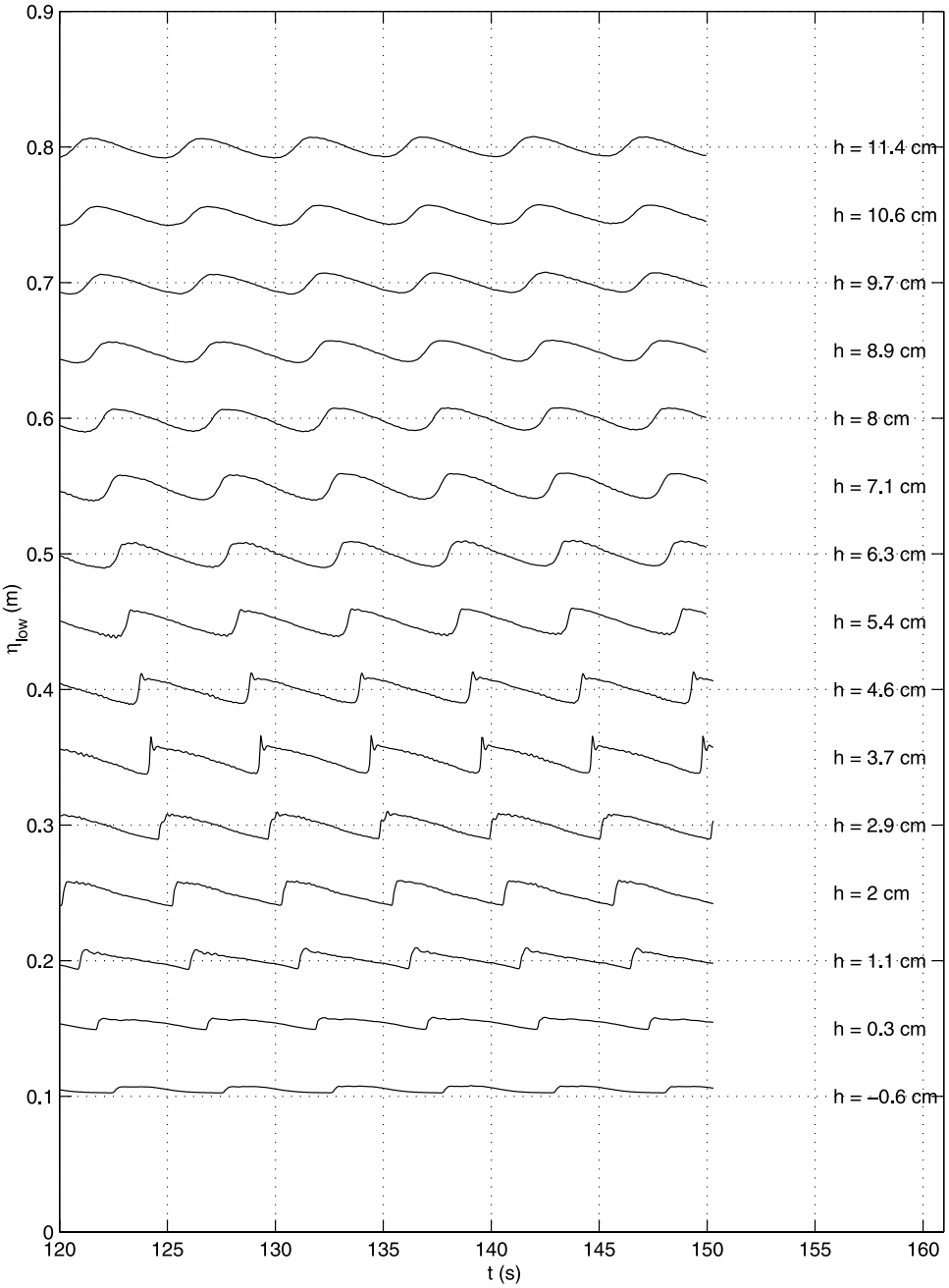

Figure 9. Time series of the total measured time series for consecutive gauge positions around the still water line for a free long wave with a frequency equal to the difference frequency of case A-1.

on the β_b parameter and varies between 0.25 and 2.0 (Figure 2). This dependency on β_b is valid for the off-resonant LF forcing, implying that the forcing short waves are not in shallow water in the shoaling zone.

[45] The reflection of long waves on the shoreline is dependent on β_H with a transition to almost full reflection at β_H = 1.25 (Figure 3). For small values of β (mild-slope regime) the LF waves appear to be breaking as they are propagating with the short waves (Figure 4). The dominant dissipation mechanism of long waves in the mild-slope regime is indeed shown to be breaking (Figure 6). We also confirm the findings of *Thomson et al.* [2006] and *Henderson et al.* [2006] that bottom friction is not the relevant dissipation agent. We find that the energy transfer from low frequencies (in the field "infragravity waves") to higher frequencies (in the field "swell") is partly due to triad interactions between IG waves and swell (as found by *Thomson et al.* [2006] and *Henderson et al.* [2006]) but is increasingly dominated by self-self interactions of the LF-waves for very shallow water (Figure 7) which cause the long-wave front to steepen up and break. This process of long-wave breaking in the near-shore zone is confirmed by laboratory observations of initially monochromatic, free long waves with the same frequency as the difference

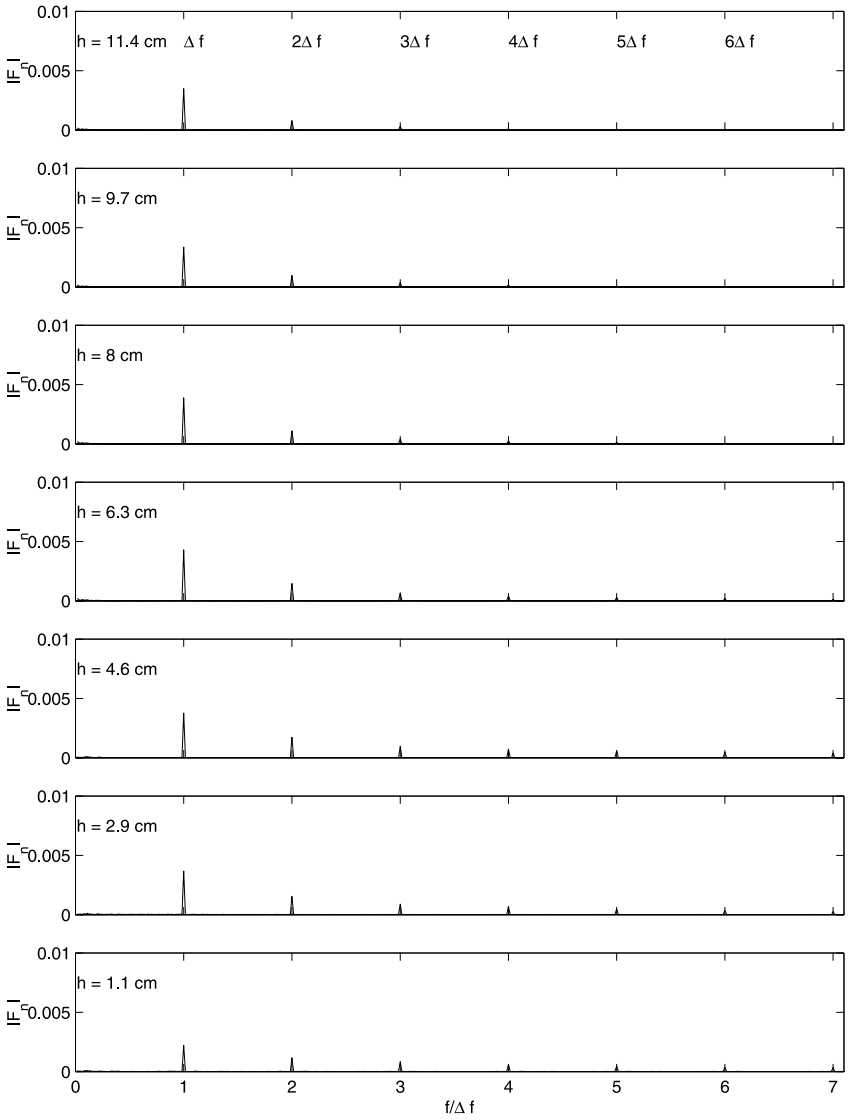

Figure 10. Frequency spectra of the free long-wave case with a frequency equal to the difference frequency of case A-1 at various depths. The most important frequency components are indicated in the first panel. The frequency axis is normalized by $\Delta f = 0.1953$ Hz.

frequency of case A-1, propagating over a plane sloping beach. The results show strikingly similar patterns of steepening and breaking of the wave (Figure 9) with a similar frequency distribution and spatial evolution (Figure 10) as in the bichromatic, forced-wave case.

Appendix A: Decomposition of Low-Frequency Waves

[46] The first step in the data analysis is to split the measured wave records in a high-frequency part (which contains the primary frequencies) and a low-frequency part (which contains the difference frequencies) using a Fourier-domain (high-pass/low-pass) filter with a cut-off frequency at half the mean frequency. After that, the low-frequency wave signal is decomposed into an incoming component traveling toward the shoreline (which is primarily "bound," since the generation of free long waves is suppressed at the wave maker) and a reflected (free) component which propagates to deeper water. This separation is done using the method described by *Battjes et al.* [2004] with modifications for shoaling and phase speed effects, which are described in this section. The method uses Fourier-transformed measured wave information from a subarray of (typically) seven adjacent wave gauges as input. The complex amplitude after transformation can be written:

$$Z_{m,p} = \frac{1}{N}\sum_{j=1}^{N} \zeta(x_p, t_j)\, e^{-i2\pi f_m t_j}, \tag{A1}$$

where $Z_{m,p}$ is the measured complex amplitude, p is the gauge number in the local array with $p = 1,\ldots,P$, with P the total number of gauges in the local array which is centered around gauge R, j is the time index, N is the total number of points in the time series, ζ is the time series of the surface elevation, and $f_m = m/D$ is the long-wave frequency, with D the duration and m the two-sided frequency counter (0, ±1, ±2, ...). This measured complex amplitude at the reference

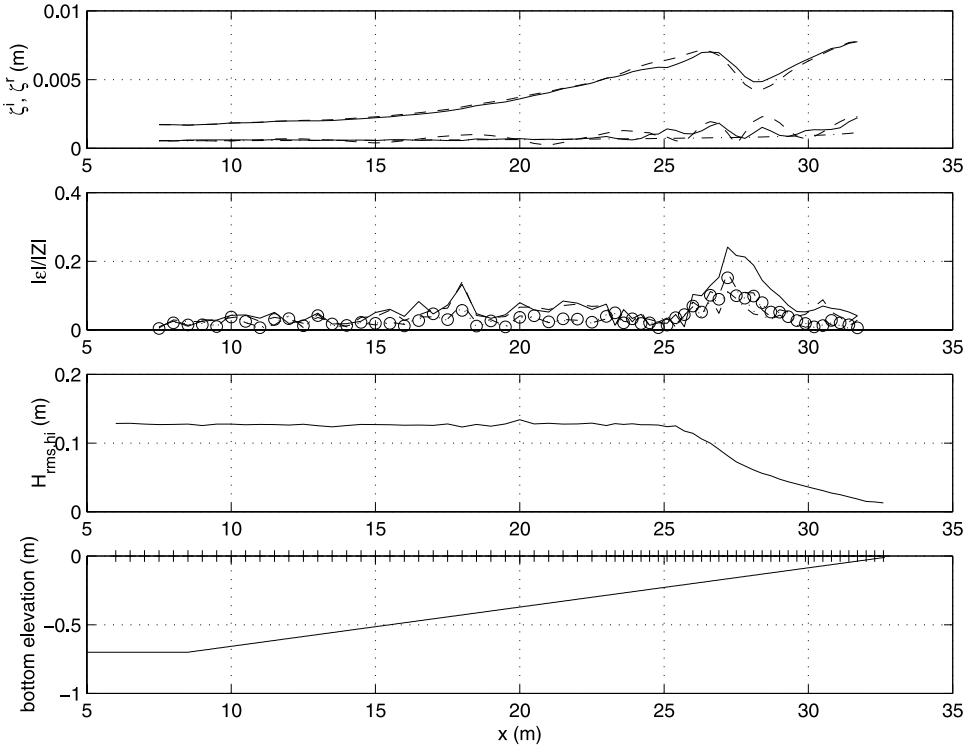

Figure A1. The first panel shows the amplitude of the incoming long wave (upper solid line) and reflected long wave (lower solid line). The initial estimate of the amplitude of the incoming and reflected long wave is shown as the upper dashed and lower dashed lines, respectively. Green's Law is shown as the dash-dotted line (reflected waves only). The second panel shows the absolute error ε normalized with the measured amplitude Z for five iterations (first step, solid line; second step, dashed line; third step, dash-dotted line; fourth step, dotted line; fifth step, circles). The third panel shows the H_{rms} of the short waves. The fourth panel shows the bathymetry and gauge locations (pluses).

gauge R is considered as the sum of an incoming wave component $Z^{(i)}_{m,R,n}$, a reflected wave component $Z^{(r)}_{m,R,n}$ and an error $\varepsilon_{m,p,n}$, written as

$$Z_{m,p} = Q^{(i)}_{m,p,n} Z^{(i)}_{m,R,n} + Q^{(r)}_{m,p,n} Z^{(r)}_{m,R,n} + \varepsilon_{m,p,n}, \tag{A2}$$

where superscript (i) indicates "incoming," superscript (r) indicates "reflected," n is a step counter in the multistep procedure (detailed below). The factors $Q^{(i)}_{m,p,n}$ and $Q^{(r)}_{m,p,n}$ are complex shoaling and phase speed correction factors, which are a function of frequency, location, center position, and iteration step.

[47] The system (A2) consists of P equations per frequency with two unknowns $Z^{(i)}_{m,R,n}$ and $Z^{(r)}_{m,R,n}$. When $P > 2$, this system is overdetermined and a solution is found using the method of least squares. The system of equations can be written as

$$\begin{bmatrix} Q^{(i)}_{m,1,n} & Q^{(r)}_{m,1,n} \\ \cdots & \cdots \\ Q^{(i)}_{m,R,n} & Q^{(r)}_{m,R,n} \\ \cdots & \cdots \\ Q^{(i)}_{m,P,n} & Q^{(r)}_{m,P,n} \end{bmatrix} \begin{bmatrix} Z^{(i)}_{m,R,n} \\ Z^{(r)}_{m,R,n} \end{bmatrix} = \begin{bmatrix} Z_{m,1} \\ \cdots \\ Z_{m,R} \\ \cdots \\ Z_{m,P} \end{bmatrix} + \begin{bmatrix} \varepsilon_{m,1,n} \\ \cdots \\ \varepsilon_{m,R,n} \\ \cdots \\ \varepsilon_{m,P,n} \end{bmatrix}. \tag{A3}$$

[48] In the first step ($n = 1$) the factors Q are set to

$$\begin{aligned} Q^{(i)}_{m,p,1} &= e^{i\Phi^{(i)}_{m,p}} \\ Q^{(r)}_{m,p,1} &= e^{i\Phi^{(r)}_{m,p}} \end{aligned}, \tag{A4}$$

where $\Phi^{(i)}_{m,p}$ and $\Phi^{(r)}_{m,p}$ are the initial estimates of the phase functions based on linear theory. The incoming long waves are initially assumed to propagate with the group speed c_g, so

$$\Phi^{(i)}_{m,p} = -\int_{x=0}^{x=x_p} \frac{2\pi f_m}{c_{g,p}} dx. \tag{A5}$$

[49] The reflected long waves are assumed to propagate with the linear phase speed c or

$$\Phi^{(r)}_{m,p} = \int_{x=0}^{x=x_p} \frac{2\pi f_m}{c_{m,p}} dx. \tag{A6}$$

[50] In this step we thus assume that the phase variation is according to the initially estimated phase variation and that there is no shoaling over the local array. This last assumption does not preclude an amplitude variation between subarrays.

[51] Solving equation (A3) yields an estimate of $Z^{(i)}_{m,R,1}$ and $Z^{(r)}_{m,R,1}$. The local array is moved one wave gauge position and the system is solved again to obtain another estimate at the new center location R. At the end of this step we have an estimate for all wave gauges (except the $(P\text{-}1)/2$ at either end of the total array) for all low frequencies m. The result can be interpreted as a quasi-continuous variation of the real amplitudes and phases because of the high resolution of the gauge spacing. Until this point the method is similar to that of *Battjes et al.* [2004].

[52] The modification is in the subsequent steps. The solution obtained in the first step is a complex amplitude, the argument of which can be interpreted as a phase correction to the originally prescribed phase at the center location of the subarray. In the second step, this phase correction of the incident waves is added to the original phase through multiplication in the complex domain by prescribing

$$\begin{aligned} Q^{(i)}_{m,p,2} &= \frac{Z^{(i)}_{m,p,1}}{|Z^{(i)}_{m,p,1}|} Q^{(i)}_{m,p,1} \\ Q^{(r)}_{m,p,2} &= Q^{(r)}_{m,p,1} \end{aligned} . \tag{A7}$$

[53] We solve the system (A3) again which yields $Z^{(i)}_{m,R,2}$ and $Z^{(r)}_{m,R,2}$ for all wave gauges as we move the local array along the total array. In effect, we add no information to the system but re-use information obtained from estimates involving multiple arrays to correct local phase speeds inside the local array. In a way, this method can be interpreted as a predictor-corrector operation.

[54] In step 3 ($n = 3$) we allow for a variation of the wave amplitudes over the local array (due to shoaling)

$$\begin{aligned} Q^{(i)}_{m,p,3} &= \frac{|Z^{(i)}_{m,p,2}|}{|Z^{(i)}_{m,R,2}|} Q^{(i)}_{m,p,2} \\ Q^{(r)}_{m,p,3} &= Q^{(r)}_{m,p,2} \end{aligned} . \tag{A8}$$

In steps 4 and 5 ($n = 4$ and $n = 5$) we do the same for the reflected wave, first correcting for the shoaling and then applying the phase correction.

[55] Using synthetic data, *Steenbergen* [2005] found that the order in which steps 2 and 3, and steps 4 and 5 are executed are not important, but they cannot be executed in one step. He also found that the method works well if in the analysis the phase variation and amplitude variation of one of the two components is known or can at least be assumed with reasonable accuracy. The method converges if the initial estimate of the unknown phase speed is not much different from the actual phase speed. For the present data set, we expect that the propagation and shoaling characteristics of the outgoing wave are accurately represented by linear theory and conservative shoaling such that the method is suitable for our present purpose. Moreover, since we anticipate that the initial estimate of the celerity of the incident bound wave (group speed corresponding to the peak frequency of the spectrum) is close to the actual speed the method will likely converge rapidly.

[56] The multistep method reduces oscillations in the estimated reflected long-wave amplitude that occur after the first decomposition step [see *Battjes et al.*, 2004; *Steenbergen*, 2005], which are thus attributed to the inaccuracies in the assumed phase speed and amplitude variation of the incoming wave in the decomposition technique [*Steenbergen*, 2005]. Also, it is found that in the shoaling zone the phase speed is adjusted slightly and is smaller than c_g consistent with the theoretical prediction by *Janssen et al.* [2003]. Until now, the oscillations in the reflected wave were interpreted as a physical phenomenon [*van Dongeren*, 1997; *Battjes et al.*, 2004] but in fact seem at least in part to be spurious. To investigate this finding is beyond the scope of this paper and will be pursued in a subsequent paper.

[57] Figure A1 shows a typical result for case A2. The fourth panel shows the bathymetry of the horizontal approach, the plane slope and the locations of the wave gauges, with the shoreline to the right. The third panel shows the wave height variation of the short waves primarily to indicate the location of the breakpoint around x = 26 m. The first panel shows the amplitude variation of the incoming wave (upper solid line) and of the reflected free wave (lower solid line). The initial estimates of the incoming and reflected wave amplitude variation are shown as the dashed lines. The figure shows that the iteration method reduces the amplitude variations of the incoming long wave in the surf zone and strongly reduces the spatial variations in the reflected wave amplitude estimates. The incoming long wave in the first panel displays shoaling outside of the breaker zone, and then a decay of wave amplitude which may result from a loss of energy due to a transfer to the short waves [*van Dongeren et al.*, 1996], which is not unlike the results found by *Baldock and O'Hare* [2004]. This negative energy transfer is later reversed and energy is gained again in the inner surf zone. The process of energy gain and loss in the surf zone is not yet fully understood and will not be addressed in this paper further. Our focus is on the phenomena in the shoaling zone and very close to the shoreline. Finally, the second panel shows the evolution of the normalized error $|\varepsilon/Z|$, which is shown to reduce in step 2 and then stay relatively constant in subsequent steps at a value of less than 5%, except at the breakpoint where it increases locally to 15%. This evolution shows that the first step is most effective in reducing the overall error and the subsequent steps redistribute the total signal over the incoming and reflected signal without reducing the overall error much.

[58] The incoming long wave is only partially reflected (about 25%) at the shoreline (Figure A1). The reflected wave amplitude (lower solid line) deshoals following Green's Law (dash-dotted line, initiated with the offshore-most reflected wave estimate and using still water to compute the shoaling) with some oscillations around this trend, which are ascribed to small remaining errors in the estimated phase speed of the incoming long wave. For small depths, the assumption of still water for computing the shoaling is not valid because of wave-induced set up which adds to the total depth. Consequently, we notice that the computed amplitudes are consistently above Green's Law in the region near the shore.

[59] **Acknowledgments.** This work was sponsored by Delft University and WL|Delft Hydraulics (ARvD) in the framework of the Netherlands Center for Coastal Research. Funding for A.R. was provided by the Dutch National Science Foundation (NWO) contract DCB.5856. We thank the technical staff of the Fluid Dynamics Laboratory at Delft University for their help in performing the experiments.

References

Baldock, T. E., and T. J. O'Hare (2004), Energy transfer and dissipation during surf beat conditions, in *Proceedings of the 29th International Conference on Coastal Engineering*, edited by J. McKee Smith, pp. 1212–1224, World Sci., Hackensack, N. J.

Baldock, T. E., D. A. Huntley, P. A. D. Bird, T. O'Hare, and G. N. Bullock (2000), Breakpoint generated surf beat induced by bichromatic wave groups, *Coastal Eng.*, *39*, 213–242.

Battjes, J. A. (1974), Surf similarity, in *Proceedings of the 14th International Conference on Coastal Engineering*, edited by B. Edge, pp. 466–480, Am. Soc. of Civ. Eng., Reston, Va.

Battjes, J. A., and J. P. F. M. Janssen (1978), Energy loss and set-up due to breaking of random waves, in *Proceedings of the 16th International Conference on Coastal Engineering*, edited by B. Edge, pp. 569–587, Am. Soc. of Civ. Eng., Reston, Va.

Battjes, J. A., H. J. Bakkenes, T. T. Janssen, and A. R. van Dongeren (2004), Shoaling of subharmonic gravity waves, *J. Geophys. Res.*, *109*, C02009, doi:10.1029/2003JC001863.

Biésel, F. (1952), Équations générales au second ordre de la houle irrégulière, *Houille Blanche*, *5*, 371–376.

Boers, M. (1996), Simulation of a surf zone with a barred beach. part 1: Wave heights and wave breaking, *Rep. 96-5*, 116 pp., Comm. on Hydrol. and Geol. Eng., Dep. of Civ. Eng., Delft Univ. of Technol., Delft, Netherlands.

Bowers, E. C. (1977), Harbour resonance due to set-own beneath wave groups, *J. Fluid Mech.*, *79*(1), 71–92.

Elgar, S., T. H. C. Herbers, M. Okihiro, J. Oltman-Shay, and R. T. Guza (1992), Observations of infragravity waves, *J. Geophys. Res.*, *97*, 15,537–15,577.

Elgar, S., T. H. C. Herbers, and R. T. Guza (1994), Reflection of ocean surface gravity waves from a natural beach, *J. Phys. Oceanogr.*, *24*, 1503–1511.

Foda, M. A., and C. C. Mei (1981), Nonlinear excitation of long-trapped wave by a group of short swells, *J. Fluid Mech.*, *111*, 319–345.

Henderson, S. M., and A. J. Bowen (2002), Observations of surf beat forcing and dissipation, *J. Geophys. Res.*, *107*(C11), 3193, doi:10.1029/2000JC000498.

Henderson, S. M., R. T. Guza, S. Elgar, T. H. C. Herbers, and A. J. Bowen (2006), Nonlinear generation and loss of infragravity wave energy, *J. Geophys. Res.*, *111*, C12007, doi:10.1029/2006JC003539.

Janssen, T. T., J. W. Kamphuis, A. R. Van Dongeren, and J. A. Battjes (2000), Observations of long waves on a uniform slope, in *Proceedings, International Conference on Coastal Engineering*, edited by B. Edge, pp. 2192–2205, Am. Soc. of Civ. Eng., Reston, Va.

Janssen, T. T., J. A. Battjes, and A. R. van Dongeren (2003), Long waves induced by short wave groups over a sloping bottom, *J. Geophys. Res.*, *108*(C8), 3252, doi:10.1029/2002JC001515.

Kamphuis, J. W. (1996), Experiments on design wave height in shallow water, in *Proceedings of the 25th International Conference on Coastal Engineering*, edited by B. Edge, pp. 221–232, Am. Soc. of Civ. Eng., Reston, Va.

Kostense, J. K. (1984), Measurements of surf beat and set-down beneath wave groups, in *Proceedings of the 19th International Conference on Coastal Engineering*, edited by B. Edge, pp. 724–740, Am. Soc. of Civ. Eng., Reston, Va.

List, J. H. (1992), A model for two-dimensional surfbeat, *J. Geophys. Res.*, *97*, 5623–5635.

Longuet-Higgins, M. S., and R. W. Stewart (1962), Radiation stress and mass transport in gravity waves with application to ''surf-beats,'' *J. Fluid Mech.*, *8*, 565–583.

Longuet-Higgins, M. S., and R. W. Stewart (1964), Radiation stress in water waves: A physical discussion with applications, *Deep Sea Res.*, *11*, 529–563.

Madsen, P. A., O. R. Sørensen, and H. A. Schäffer (1997), Surf zone dynamics simulated by a Boussinesq type model. part II: Surf beat and swash oscillation for wave groups and irregular waves, *Coastal Eng.*, *32*, 289–319.

Masselink, G. (1985), Group bound long waves as a source of infragravity energy in the surf zone, *Cont. Shelf Res.*, *15*(13), 1525–1547.

Munk, W. H., and M. Wimbush (1969), A rule of thumb for wave breaking over sloping beaches, *Oceanology*, Engl. Transl., *9*, 56–59.

Nazaka, E., S. Tsukayama, and M. Hino (1990), Bore-like surf beat on reef coasts, in *Proceedings of the 22nd International Conference on Coastal Engineering*, edited by B. Edge, pp. 743–756, Am. Soc. of Civ. Eng., Reston, Va.

Okihiro, M., and R. T. Guza (1995), Infragravity energy modulation by tides, *J. Geophys. Res.*, *100*, 16,143–16,148.

Putnam, J. A., and J. W. Johnson (1949), The dissipation of wave energy by bottom friction, *Eos Trans. AGU*, *30*, 67–74.

Roelvink, J. A. (1993), Surfbeat and its effect on cross-shore profiles, Ph.D. dissertation, Delft Univ. of Technol., Delft, Netherlands.

Ruessink, B. G., M. G. Kleinhans, and P. G. L. van den Beukel (1998), Observations of swash under highly dissipative conditions, *J. Geophys. Res.*, *103*, 3111–3118.

Ruessink, B. G., D. J. R. Walstra, and H. N. Southgate (2003), Calibration and verification of a parametric wave model on barred beaches, *Coastal Eng.*, *48*, 139–149.

Ruggiero, P., R. A. Holman, and R. A. Beach (2004), Wave run-up on a high-energy dissipative beach, *J. Geophys. Res.*, *109*, C06025, doi:10.1029/2003JC002160.

Schäffer, H. A., and I. A. Svendsen (1988), Surf beat generation on a mild slope beach, in *Proceedings of the 21st International Conference on Coastal Engineering*, edited by B. Edge, pp. 1058–1072, Am. Soc. of Civ. Eng., Reston, Va.

Sénéchal, N., P. Bonneton, and H. Dupuis (2001), Field observations of irregular wave transformation in the surf zone, in *Coastal Dynamics '01*, pp. 62–71, Am. Soc. of Civ. Eng., Reston, Va.

Sheremet, A., R. T. Guza, S. Elgar, and T. H. C. Herbers (2002), Observations of nearshore infragravity waves: 1. Seaward and shoreward propagating components, *J. Geophys. Res.*, *107*(C8), 3095, doi:10.1029/2001JC000970.

Steenbergen, G. J. A. M. (2005), Bi-directional decomposition of subharmonic gravity waves, M. S. thesis, 117 pp., Delft Univ. of Technol., Delft, Netherlands. (Available at http://www.citg.tudelft.nl/live/binaries/4de0d195-5207-4e67-84bb-455c5403ae47/doc/2005Steenbergen.pdf)

Steenhauer, K. (2003), Numerical modelling of surfbeat, M. S. thesis, 94 pp., Delft Univ. of Technol., Delft, Netherlands. (Available at http://www.citg.tudelft.nl/live/binaries/4de0d195-5207-4e67-84bb-455c5403ae47/doc/2003Steenhauer.pdf)

Swart, D. H. (1974), Offshore sediment transport and equilibrium beach profiles, *Publ. 131*, Delft Hydraul. Lab., Delft, Netherlands.

Symonds, G., D. A. Huntley, and A. J. Bowen (1982), Two dimensional surf-beat: Long wave generation by a time-varying break point, *J. Geophys. Res.*, *87*, 492–498.

Thomson, J., S. Elgar, B. Raubenheimer, T. H. C. Herbers, and R. T. Guza (2006), Tidal modulation of infragravity waves via nonlinear energy losses in the surfzone, *Geophys. Res. Lett.*, *33*, L05601, doi:10.1029/2005GL025514.

van Dongeren, A. R. (1997), Quasi 3-D modeling of nearshore hydrodynamics, *Rep. CACR-97-04*, 243 pp., Cent. for Appl. Coastal Res., Univ. of Del., Newark.

van Dongeren, A. R., I. A. Svendsen, and F. E. Sancho (1996), Generation of infragravity waves, in *Proceedings of the 25th International Conference on Coastal Engineering*, edited by B. Edge, pp. 1335–1348, Am. Soc. of Civ. Eng., Reston, Va.

van Dongeren, A. R., H. J. Bakkenes, and T. T. Janssen (2002), Generation of long waves by short wave groups, in *Proceedings of the 28th International Conference on Coastal Engineering*, edited by J. McKee Smith, pp. 1093–1105, World Sci., Hackensack, N. J.

van Dongeren, A. R., J. van Noorloos, K. Steenhauer, J. A. Battjes, T. T. Janssen, and A. Reniers (2004), Shoaling and shoreline dissipation of subharmonic gravity waves, in *Proceedings, International Conference on Coastal Engineering*, edited by J. McKee Smith, pp. 1225–1237, World Sci., Hackensack, N. J.

van Noorloos, J. C. (2003), Energy transfer between short wave groups and bound long waves on a plane slope, M. S. thesis, 68 pp., Delft Univ. of Technol., Delft, Netherlands. (Available at http://www.citg.tudelft.nl/live/binaries/4de0d195-5207-4e67-84bb-455c5403ae47/doc/2003vanNoorloos.pdf)

Wright, L. D., J. Chappell, B. G. Thom, M. P. Bradshaw, and P. Cowell (1979), Morphodynamics of reflective and dissipative beaches and inshore systems: Southeastern Australia, *Mar. Geol.*, *32*, 105–140.

J. Battjes, A. Reniers, and G. Steenbergen, Section of Environmental Fluid Mechanics, Department of Civil Engineering, Delft University of Technology, Stevinweg 1, NL-2628 CN Delft, Netherlands.

T. Janssen, Department of Oceanography, Naval Postgraduate School, 833 Dyer Road, Monterey, CA 93943-5122, USA.

K. Steenhauer, Department of Engineering, King's College, University of Aberdeen, Aberdeen AB24 3UE, UK.

A. van Dongeren, WL|Delft Hydraulics, P. O. Box 177, NL-2600 MH Delft, Netherlands. (ap.vandongeren@wldelft.nl)

J. van Noorloos, Vopak, Koningin Wilhelminahaven ZOZ 1, NL-3134 KH Vlaardingen, Netherlands.